frontiers | Frontiers in Materials

TYPE Original Research
PUBLISHED 10 September 2025
DOI 10.3389/fmats.2025.1629892

OPEN ACCESS

EDITED BY
Jiangyu Wu,
China University of Mining and Technology, China

REVIEWED BY
Guojian Liu,
Suzhou University of Science and Technology, China
Syahrul Fithry Senin,
Universiti Teknologi Teknologi MARA, Malaysia

*CORRESPONDENCE
Duoxi Yao,
dxyao@aust.edu.cn

RECEIVED 16 May 2025
ACCEPTED 06 June 2025
PUBLISHED 10 September 2025

CITATION
Shi G, Yao D, Wu J and Meng F (2025) Experimental study on dynamic characteristics and energy dissipation of weakly cemented rock-like materials. *Front. Mater.* 12:1629892. doi: 10.3389/fmats.2025.1629892

Experimental study on dynamic characteristics and energy dissipation of weakly cemented rock-like materials

Guodong Shi[1], Duoxi Yao[1]*, Jiehao Wu[2,3] and Fangyi Meng[2]

[1]School of Earth and Environment, Anhui University of Science and Technology, Huainan, China, [2]National-Local Joint Engineering Laboratory of Building Health Monitoring and Disaster Prevention Technology, Anhui Jianzhu University, Hefei, China, [3]School of Civil Engineering and Architecture, Anhui University of Science and Technology, Huainan, China

The structural stability of coal seam roof rock mass under dynamic load in engineering practice is directly influenced by the dynamic characteristics of weakly consolidated coal measures rock. A study was conducted on two types of rocks, mudstone and siltstone, around the roof of coal seam No. 31 in Renlou Coal Mine, northern Anhui Province. Rock-like specimens were created using similar materials for analysis. The mechanical properties, energy dissipation characteristics, and fractal characteristics of these rocks were investigated using a 75 mm Split Hopkinson Pressure Bar (SHPB) test system at five different impact velocities. The findings are as follows: 1) As the impact velocity increases, the strain rate of the rock linearly increases while the dynamic uniaxial compressive strength exponentially increases. 2) With an increase in strain rate, there is a negative correlation between rock fragmentation and a positive correlation with the number of fragments produced; additionally, the fractal dimension shows an increasing quadratic term function relationship. 3) There exists a linear positive correlation between incident energy and impact velocity; moreover, as incident energy increases, so does the amount of energy lost due to rock breakage. These research results provide both theoretical and experimental foundations for mine dynamic disaster protection.

KEYWORDS

weakly consolidated rock, strain rate effect, dynamic response, energy dissipation, fractal characteristic

1 Introduction

Coal plays a strategic role in China's economic development system and holds a crucial position in the energy structure (Li and Yuan, 2023; Wang S. M. et al., 2022; Kang et al., 2023; Wu et al., 2025; Xie et al., 2022; Wu J. Y. et al., 2024). As coal resources mining transitions to deeper formations, the deep formation rocks exhibit characteristics of "three heights and one disturbance" (Shu et al., 2023; Yang et al., 2024; Zheng Q. Q. et al., 2024; Shi et al., 2024; Shi et al., 2025), leading to a complex stress state and frequent dynamic disasters such as rock bursts, floor protrusions, and roof cavings (Hao et al., 2022; Gong et al., 2023; Hu et al., 2023; Tan et al., 2024; Zheng Q. et al., 2024; Lyu et al., 2022; Deng et al., 2023). Engineering disasters like large deformations, high ground pressures, and challenging roadway support under dynamic

TABLE 1 Mechanical properties of the overlying roof in coal seams No. 3_1 ($\frac{min-max}{mean}$).

Rock	Compressive strength (MPa)	Tensile strength (MPa)	Shear strength (MPa)		Elasticity modulus (GPa)	Poisson ratio
			Internal friction angle	Cohesive force		
Mudstone	6.97–66.68 17.44	0.80–5.39 1.17	29°40′-37°41′ 33°01′	0.82–4.75 1.75	0.86–3.93 2.04	0.17–0.30 0.22
Siltstone	12.54–112.90 28.64	1.24–4.47 2.19	35°05′-38°33′ 36°37′	1.28–3.71 2.22	1.99–3.62 2.80	0.15–0.22 0.19

TABLE 2 The ratio between two analogous rock materials.

Similar material	Proportion
Siltstone-like material	Concrete: Quartz sand: Water = 1.00:0.88:0.45
Mudstone-like material	Concrete: Quartz sand: Gypsum: Water = 1.00:0.80:0.20:0.55

loading are on the rise (Zhang et al., 2019; He et al., 2024; Yin et al., 2024). Blasting is a significant method for coal mine rock roadway excavation and forced caving (Yue et al., 2022; Zhou K. et al., 2022; Yang et al., 2023; Cheng et al., 2024; Zuo et al., 2024; Zhao et al., 2025; Liao et al., 2025; Zhang et al., 2025; Li et al., 2025; Zheng et al., 2025). Therefore, it is imperative to analyze and summarize the mechanical characteristics of coal seam roof rocks under dynamic actions to ensure the safe mining of coal and rock.

In recent years, SHPB has gained significant traction in investigating the dynamic mechanical properties of rock materials under medium and high strain rates. Shi (Shi et al., 2023a; Shi et al., 2023b) based on observations from SHPB test results, proposed new concepts of internal cohesion and internal friction angle for quantitative analysis of the pre-peak and post-peak stages of the dynamic loading process of sandstone. Rae et al. (Rae et al., 2020; Zuo et al., 2022; Fang S. et al., 2023; Sun et al., 2023; Wu et al., 2023) conducted SHPB impact compression tests on both soft rock and hard rock, and found a significant correlation between strain rate and rock strength. Additionally, the study revealed that rock strength decreases significantly with an increase in fractal dimension. Liu et al. (Liu et al., 2022; Wang X. et al., 2022; You et al., 2022; Zhou T. et al., 2022; Wen et al., 2023; Xia et al., 2023; Zheng et al., 2023; Gao et al., 2024; Wu J. H. et al., 2024) conducted dynamic splitting experiments on brittle rock and discovered a highly significant linear positive correlation between the dynamic tensile strength and the loading rate. Moreover, it was observed that the failure of rock specimens initiated from internal defects, with changes in geometric characteristics of these defects influencing the fracture mode. Numerous researchers (Yuan et al., 2022; Zhou J. et al., 2022; Lyu et al., 2023; Wang et al., 2023; Zhao et al., 2023; Wang et al., 2021; Zhang et al., 2021) have conducted impact fracture experiments on rock samples and found that the energy dissipation characteristics of rock samples are related to the distribution of fragment sizes, and various efficiency indicators have been proposed to represent the crushing efficiency under different conditions.

The dynamic behavior of weakly cemented rocks, in particular, is a critical concern due to their inherent instability. Studies on materials like weakly cemented red sandstone (Fang S. Z. et al., 2023) and argillaceous weakly cemented rock (Meng et al., 2020) have highlighted their strain rate sensitivity and unique energy absorption patterns under dynamic loads. The deformation and failure of rock-like materials is essentially a process of energy dissipation (Chen et al., 2022), making the study of energy transformation and dissipation mechanisms crucial for understanding their response to impact loads and for assessing the stability of engineering rock masses. For instance, comprehensive studies on other rock types like sandstone, such as those by Yuan et al. (Yuan et al., 2024), have detailed how factors like environmental conditions (e.g., acidic drying-wetting cycles) and loading parameters affect fragmentation and energy dissipation characteristics, providing a methodological benchmark for rock dynamic studies.

The on-site sampling, transport, and processing of intact rock specimens from deep, weakly cemented coal seam roof levels are often difficult, complex, and have a low success rate due to the friable nature of these materials (Sun et al., 2019). While the aforementioned studies (Shi et al., 2023a; Shi et al., 2023b; Rae et al., 2020; Zuo et al., 2022; Fang S. et al., 2023; Sun et al., 2023; Wu et al., 2023; Liu et al., 2022; Wang X. et al., 2022; You et al., 2022; Zhou T. et al., 2022; Wen et al., 2023; Xia et al., 2023; Zheng et al., 2023; Gao et al., 2024; Wu J. H. et al., 2024; Yuan et al., 2022; Zhou J. et al., 2022; Lyu et al., 2023; Wang et al., 2023; Zhao et al., 2023; Wang et al., 2021; Zhang et al., 2021) and newer investigations (Yuan et al., 2024); Wang et al. (Fang S. Z. et al., 2023) provide valuable insights into the dynamic behavior of various rock types, including some naturally occurring weakly cemented rocks, a specific gap exists. There is a pressing need for systematic investigations into the dynamic characteristics and energy dissipation of analogous materials specifically fabricated to represent the properties of problematic weakly cemented strata, such as the mudstone and friable sandstone encountered in particular coal seam roofs. Research that directly compares the dynamic response, failure modes, and energy dissipation patterns of different types of analogous weakly cemented rock-like materials under controlled impact conditions is less common. This limits the direct applicability of findings to engineering scenarios where such specific, difficult-to-sample, weakly cemented rocks dominate.

TABLE 3 Mechanical parameters of similar materials.

Similar material	Compressive strength (MPa)	Tensile strength (MPa)	Shear strength (MPa)		Elasticity modulus (GPa)	Poisson ratio
			Internal friction angle	Cohesive force		
Mudstone-like material	12.74	1.57	31°08′	1.13	1.75	0.27
Siltstone-like material	27.05	2.32	36°00′	1.44	2.18	0.21

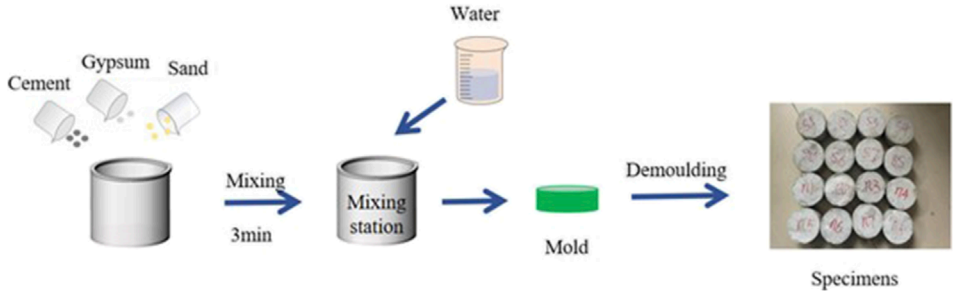

FIGURE 1
Preparation procedure for rock-like specimens.

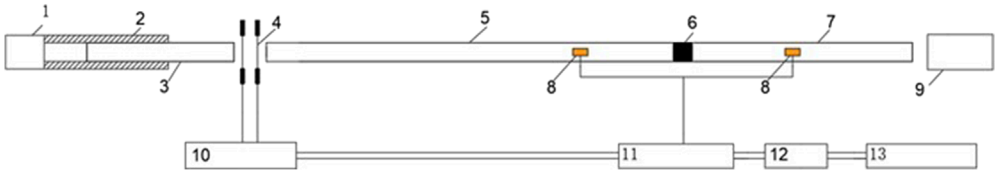

FIGURE 2
(Wu J. H. et al., 2024): 1-Plenum chamber, 2-Emission cavity, 3-Impact bar, 4-Laser source, 5-Input bar, 6-Specimen, 7-Transmission bar, 8-Strain gauge, 9-Damper, 10-Speed measuring device system, 11-Ultra-dynamic strain gauge, 12-Oscillograph, 13-Data processing system.

To address this issue, the study employs the method of fabricating analogous specimens, conducting SHPB compression experiments to evaluate the mechanical properties and failure modes of mudstone and friable sandstone specimens under impact loading to provide theoretical support for safeguarding the No. 31 coal seam roof.

2 Impact testing of weakly cemented rock-like materials

2.1 Preparation of specimens

The rock sample investigated was obtained from the mudstone-siltstone interlayer roof of coal seam No. 31 in Renlou Coal Mine, located at the intersection of Suixi County, Huaibei City and Mengcheng County, Bozhou City, Anhui Province. In order to ensure the authenticity of the simulation test, a rock sample collected from the site was meticulously cut and polished into a standardized specimen measuring Φ50 mm × 100 mm, followed by comprehensive physical and mechanical property testing. The detailed results of these tests are presented in Table 1.

Based on extensive research conducted by scholars (Wang et al., 2006; Wang et al., 2024) and in conjunction with the precise measurement of mechanical properties of roof rock from seam No. 31 in Renlou Coal Mine, the proportion of the composition of the corresponding rock-like material produced by mixing is shown in Table 2. Subsequently, the analogous materials were fabricated using the established mix ratio. The static mechanical properties of the rock-like materials were evaluated using the electronic universal testing machine located at the School of Civil Engineering, Anhui Jianzhu University. The specimen dimensions were Φ50 mm × 100 mm. The comprehensive static mechanical properties were systematically documented in Table 3. The mold used in this test has an internal size of Φ70 mm × 35 mm, and the resulting specimens are suitable for direct use in impact testing, as depicted in Figure 1.

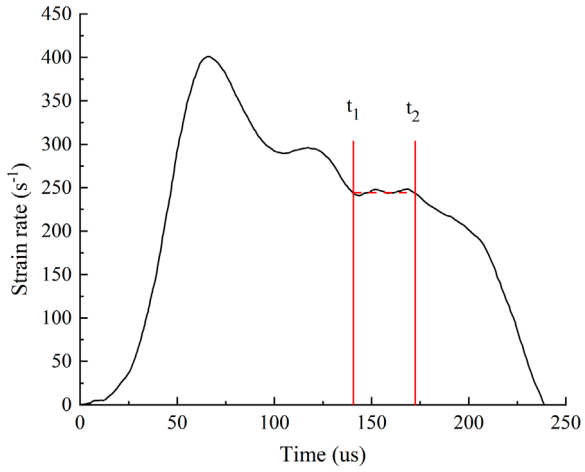

FIGURE 3
Method of strain rate determination.

2.2 Experimental apparatus and underlying principles

The test was conducted at the National-local joint Engineering Laboratory of building health monitoring and disaster prevention technology, Anhui Jianzhu University. The SHPB equipment (model: ZLKJ-SHPB-75) as shown in Figure 2 (Zuo et al., 2022). The incident rod, transmission rod, and bullet have lengths of 3000mm, 2500mm, and 500 mm respectively; their diameter is 75 mm. Additionally, the elastic modulus is measured as 206 GPa with a density of 7820 kg/m^3 and Poisson ratio of 0.29.

The SHPB impact test fulfills the assumptions of one-dimensional stress wave propagation and uniform stress distribution. The voltage signal acquired from the strain gauge is converted into a strain signal, and using the three-wave method (as Formulas 1–3) to calculate the stress $\sigma(t)$, strain $\varepsilon(t)$, and strain rate $\dot{\varepsilon}(t)$ of specimen (Zhu et al., 2009).

$$\sigma(t) = \frac{AE}{A_s}\varepsilon_t(t) \tag{1}$$

$$\varepsilon(t) = -\frac{2C_O}{L_S}\varepsilon_r(t) \tag{2}$$

$$\dot{\varepsilon}(t) = -\int_0^t \frac{2C_O}{L_S}\varepsilon_r(t)dt \tag{3}$$

where E represents the elastic modulus of the bar material; A represents the cross-sectional area of the bar material; C_o represents the longitudinal wave velocity of the bar material, and $C_O = \sqrt{E/\rho}$; L_s represents the thickness of the sample; and t represents the stress wave loading time during the test.

The SHPB impact test adheres to the assumption of one - dimensional stress waves. Specifically, it is assumed that the propagation speed of stress waves in each rod remains constant. However, in the experiment, a significant issue arises: low - frequency stress waves propagate at a relatively faster rate compared to high - frequency stress waves. This phenomenon results in oscillations in the stress - strain curves obtained during the experiment. As a consequence, accurately evaluating the mechanical properties of materials becomes challenging, a phenomenon known as the dispersion effect.

To mitigate wave dispersion and maintain a state of constant strain rate deformation in the specimen, a wave shaper made of rubber is affixed to the end of the incident rod where it is struck by the bullet. Moreover, researchers uniformly apply a layer of vaseline at the interface between the specimen and the rods. This vaseline layer serves as a lubricant, effectively reducing the adverse influence of end - friction effects on the experimental results (Wang X. et al., 2022). Simultaneously, the specimens we fabricated have dimensions of Φ70 mm × 35 mm, with the ratio of length to radius being 2:1. This ratio is close to the optimal length - to - diameter ratio ($\sqrt{3}/2$)) for specimens used in SHPB impact tests, enabling the minimization of end - friction effects and inertial effects (Wang X. et al., 2022).

2.3 Experimental design and results

The test involved the selection of five different impact pressure levels, namely, 0.10MPa, 0.13MPa, 0.15MPa, 0.18 MPa and 0.20MPa, for impacting similar specimens of mudstone and siltstone. Each group underwent three replicate experiments. After identifying and excluding outliers, a representative test value was selected from the remaining dataset.

The strain rate at the plateau is determined as the mean strain rate of the rock in this test, when the strain rate-time curve reaches a steady state (Wu J. H. et al., 2024). The data processing method is illustrated in Figure 3, and the final test results are presented in Table 4.

3 Analysis of test results

3.1 Dynamic stress-strain curve analysis

The dynamic stress-strain curve of the weakly cemented rock-like material specimen is depicted in Figure 4. For both mudstone-like material and siltstone-like material, the general trend of the curve follows an initial rise, reaching a peak, and then declining. During the initial stage of stress growth, the majority of curve segments exhibit linear elastic behavior, indicating a certain degree of positive correlation between them. The specimen also attains a state of uniform stress and strain. However, at this juncture, the stress level is insufficient to induce crack expansion in the rock specimen; instead, it can only propagate minimally along existing micro-cracks. The elastic modulus observed during this stage can serve as an appropriate dynamic elastic modulus for mudstone and siltstone. With the escalation of stress, micro-cracks progressively propagate and new cracks emerge, which are not interconnected with the primary cracks, leading to a transition into plastic deformation. As stress continues to intensify, crack propagation accelerates rapidly and microcracks link up with the main crack. During this stage, there is a change in slope on the stress-strain curve indicating a non-linear relationship until reaching peak stress. Subsequently, the slope of the stress-strain curve decreases due to macroscopic failure caused by rock cracking, resulting in diminished load-bearing capacity.

TABLE 4 The dynamic impact test results of rock-like specimens.

Similar material	Impact pressure (MPa)	Impact speed (m/s)	Strain rate (s^{-1})	Dynamic compressive strength (MPa)
Mudstone-like material	0.10	5.73	149.17	23.07
	0.13	9.35	166.88	26.51
	0.15	11.17	217.60	29.82
	0.18	13.03	256.53	34.90
	0.20	14.64	315.92	37.36
Siltstone-like material	0.10	7.17	116.36	29.50
	0.13	9.56	146.47	38.67
	0.15	10.77	182.31	52.72
	0.18	12.95	226.83	71.36

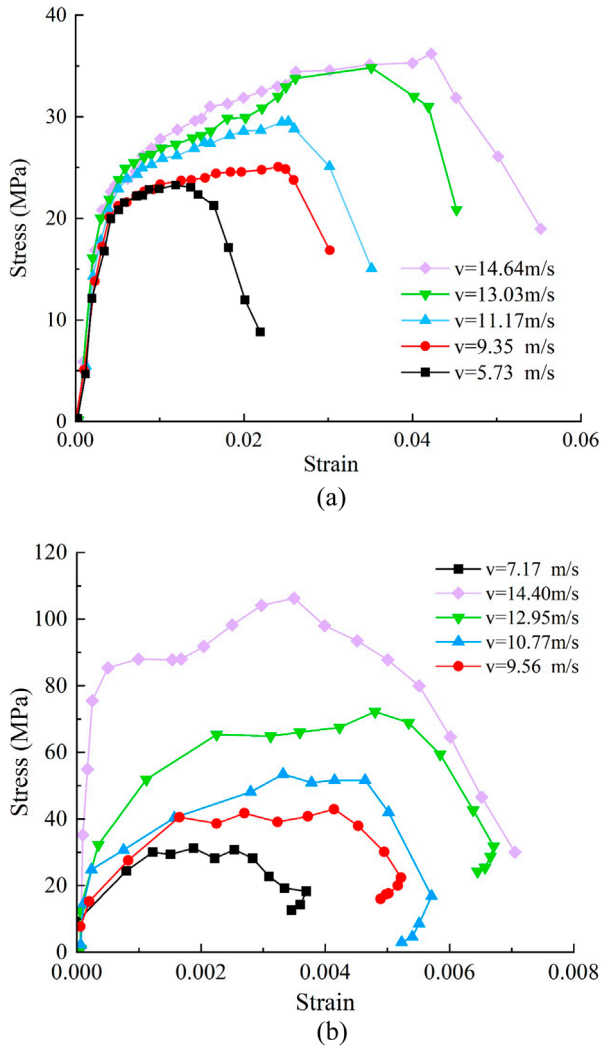

FIGURE 4
Typical dynamic stress-strain curve: **(a)** mudstone-like material, **(b)** siltstone-like material.

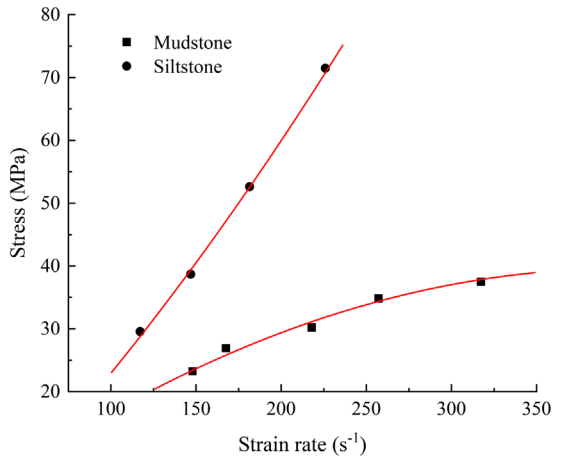

FIGURE 5
The relationship between dynamic compressive strength and strain rate.

TABLE 5 The relationship between compressive strength under dynamic loading and strain rate.

Rock	Formula	A	B	C	R^2
Mudstone	$\sigma_{bc} = A + Be^{Cx}$	46.04924	−54.23277	−0.00587	0.99969
Siltstone		−285.78	274.94	0.00115	0.99976

Compared to the curves of siltstone-like material and mudstone-like material, the stress interval of siltstone-like material is larger, indicating its superior hardness and dynamic impact resistance compared to mudstone. This trend becomes more pronounced with increasing speed. Additionally, the stress flattening stage of mudstone is brief and immediately declines after reaching its peak, whereas siltstone exhibits a prolonged period of stress flattening following the peak. Moreover, the flattening stage in siltstone shows

TABLE 6 Calculation results for the dynamic impact energy of Similar material.

Similar material	Impact pressure (MPa)	Impact speed (m/s)	Strain rate (s^{-1})	Incident energy (J)	Reflected energy (J)	Transmitted energy (J)	Dissipated energy (J)
Mudstone-like material	0.10	5.73	149.17	48.1	40.2	1.4	6.5
	0.13	9.35	166.88	73.1	58.2	2.7	12.2
	0.15	11.17	217.60	97.6	75.5	3.4	18.7
	0.18	13.03	256.53	128.3	95.3	3.9	29.1
	0.20	14.64	315.92	161.1	117.8	5.8	37.5
Siltstone-like material	0.10	7.17	116.36	37.2	28.4	2.1	6.7
	0.13	9.56	146.47	81.3	61.9	3.8	15.6
	0.15	10.77	182.31	91.4	63.5	8.2	19.7
	0.18	12.95	226.83	129.7	86.7	11.9	32.1
	0.20	14.40	329.62	151.9	101.2	9.4	41.3

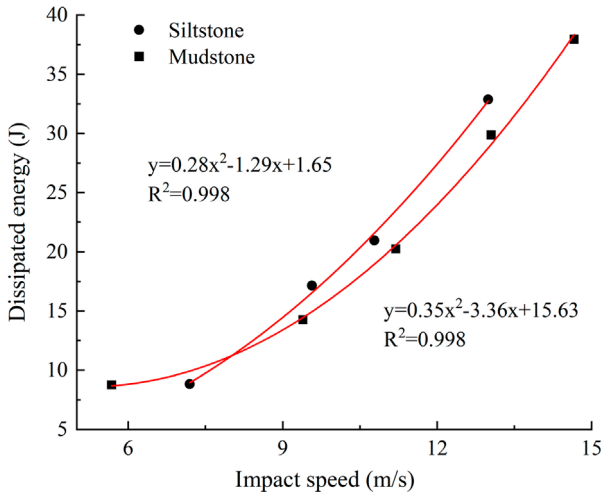

FIGURE 6
The relationship between impact velocity and dissipated energy.

a significant increase and gentler decline compared to that observed in mudstone. These observations can be attributed to the fact that siltstone does not undergo immediate destruction after reaching its stress peak, highlighting its higher yield strength when compared to mudstone.

3.2 Dynamic compressive strength analysis

The dynamic compressive strength of rocks directly reflects their resistance to external impact loads. Figure 5 and Table 5 illustrate the relationship between the dynamic compressive strength of specimens and the strain rate. It is observed that weakly cemented materials tend to harden at higher strain rates, exhibiting exponential growth beyond a certain threshold.

The two materials exhibit distinct disparities. The dynamic compressive strength of mudstone demonstrates a gradual and relatively stable growth trend with an increase in strain rate, owing to its soft nature and limited strength. Conversely, siltstone material displays an overall growth pattern that is notably faster, as evidenced by the transition of the relationship function's B value from negative to positive.

3.3 Energy dissipation relationship analysis

The bullet impacts the incident bar with a specific velocity, resulting in the transfer of impact kinetic energy carried by the bullet, as follows:

$$W_b = \frac{1}{2}mv_0^2 \tag{4}$$

where W_b represents the impact kinetic energy of a bullet, J; m represents the mass of the bullet, kg; and v_0 represents the impact velocity, m/s.

The energy carried by the incident stress wave is as follows:

$$W = A_e E_e C_e \int_0^t \varepsilon^2(t)dt \tag{5}$$

where A_e represents the cross-sectional area of the press bar, m^2; E_e represents the elastic modulus of bar; C_e represents the longitudinal wave velocity; and $\varepsilon(t)$ represents the strain corresponding to the stress wave during the loading time.

The calculation formula for incident energy W_I, transmitted energy W_T, and reflected energy W_R during the test is as follows:

$$W_I = A_e E_e C_e \int_0^t \varepsilon_I^2(t)dt \tag{6}$$

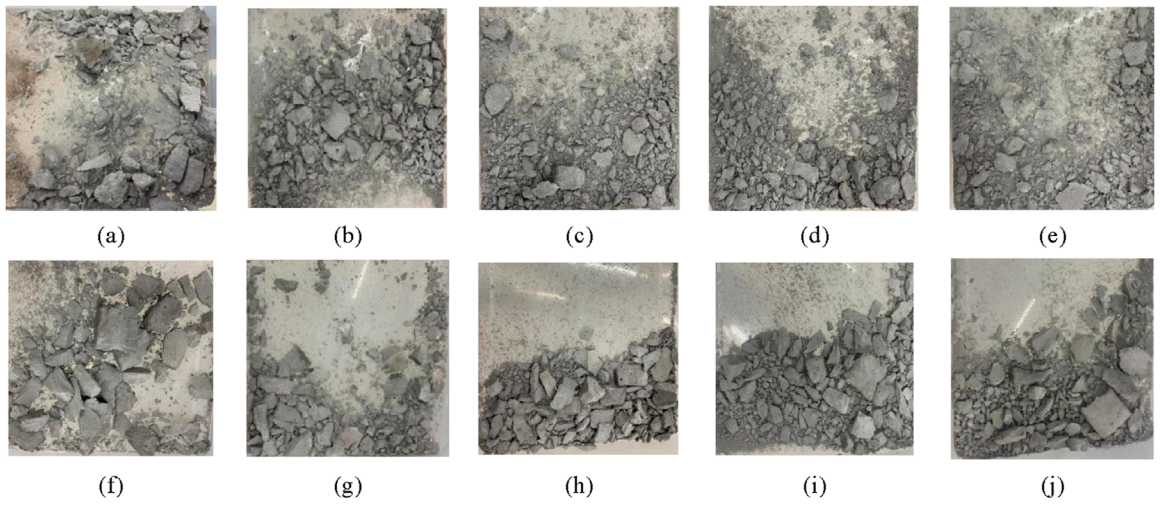

FIGURE 7
The failure patterns of specimens at different impact velocities: **(a)** Mudstone-like material, p = 0.10MPa, **(b)** Mudstone-like material, p = 0.13MPa, **(c)** Mudstone-like material, p = 0.15MPa, **(d)** Mudstone -like material, p = 0.18MPa, **(e)** Mudstone -like material, p = 0.20MPa, **(f)** Siltstone-like material, p = 0.10MPa, **(g)** Siltstone-like material, p = 0.13MPa, **(h)** Siltstone-like material, p = 0.15MPa, **(i)** Siltstone-like material, p = 0.18MPa, **(j)** Siltstone-like material, p = 0.20 MPa.

$$W_R = A_e E_e C_e \int_0^t \varepsilon_R^2(t)dt \tag{7}$$

$$W_T = A_e E_e C_e \int_0^t \varepsilon_T^2(t)dt \tag{8}$$

where $\varepsilon_I(t)$ represents the incident wave; $\varepsilon_R(t)$ represents the reflected wave; and $\varepsilon_T(t)$ represents the transmission wave of strain.

Dissipation energy of the test specimen equals incident wave energy minus reflected and transmitted wave energies, as follows:

$$W_D = W_I - (W_R + W_T) \tag{9}$$

The incident energy, reflected energy, and dissipated energy of the two rocks were computed using formulas 4–9, and the corresponding results are presented in Table 6.

The dissipated energy of rocks exhibits a velocity-dependent effect on impact. As the impact velocity increases, the dissipated energy of rocks also increases. A strong quadratic linear correlation exists between the dissipated energy of mudstone and siltstone and the impact velocity. This can be attributed to the fact that both the development and penetration of internal micro-cracks during specimen impacts require energy consumption, with higher energy consumption observed during crack generation compared to their subsequent development and penetration processes. Consequently, when subjected to low external impacts, minimal energy is generated resulting in tiny cracks within the specimen. At this stage, both absorbed energy by the specimen and its degree of damage remain low. However, as impact velocity rises, so does the generated energy which activates cracks requiring more substantial amounts of energy until complete fracture occurs in specimens (as depicted in Figure 6).

3.4 Failure blocks analysis

The failure morphology of the specimen under different impact velocities is illustrated in Figure 7. As can be seen from the figure, the mudstone specimen has been completely broken under the impact pressure of 0.10MPa, with uneven distribution of fragments. The siltstone specimen was completely broken under the impact pressure of 0.13MPa, and the fragment distribution was relatively uniform, which was basically large particle size and larger than mudstone. When the impact pressure increased to 0.18MPa, there were almost no large particle size fragments, and small particle size fragments began to appear in a large area. Compared with mudstone and siltstone, the fragmentation degree of siltstone is stronger than that of mudstone under similar impact strength.

The failure mode of rock changes from tensile failure to tension-shear coupling failure with the increase in impact velocity. In order to analyze the impact of velocity on the degree of damage in mudstone and siltstone, a statistical analysis of rock fragments was conducted following the impact test. Building upon Wang Chun's method (Gao et al., 2024) for measuring rock fragment size, it is noted that when fragmentation is minimal, its statistical significance becomes less pronounced. Therefore, a standard length greater than 35 mm was adopted for broken rock fragments and subsequent counting. The relationship between the number of damaged rock blocks, the maximum length of rock blocks, and the impact velocity is illustrated in Figure 8.

The analysis of Figure 8 reveals that the number of rock blocks with a block size greater than 35 mm exhibits a quadratic relationship with increasing impact velocity. Simultaneously, the maximum length of broken rock blocks demonstrates a quadratic decrease as impact velocity increases, indicating a reduction in

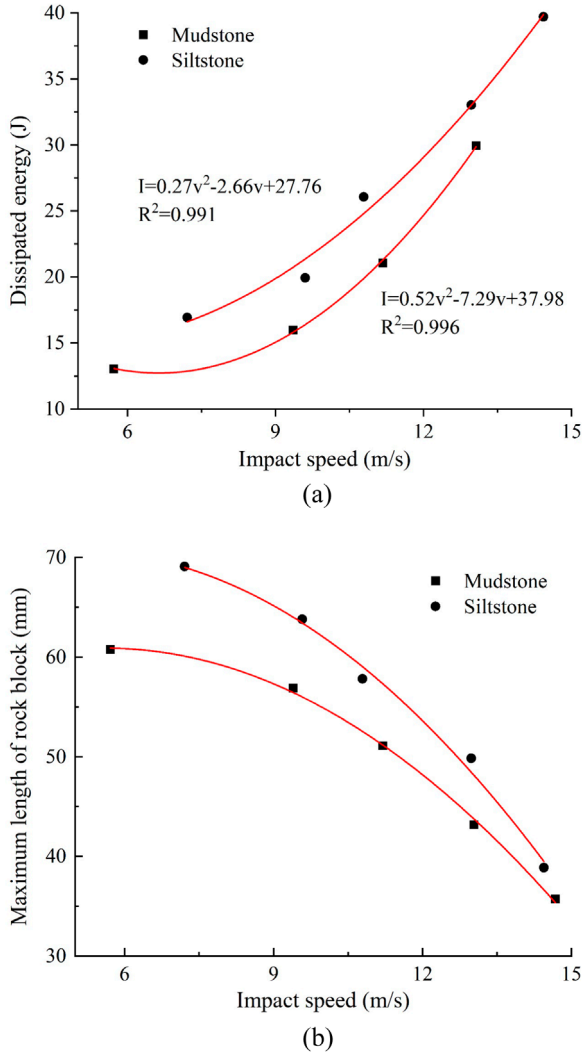

FIGURE 8
The relationship among the quantity of damaged rock mass, the maximum length of rock mass, and the impact velocity: **(a)** Quantity and impact velocity of the damaged rock mass, **(b)** Maximum length of a rock block and impact velocity.

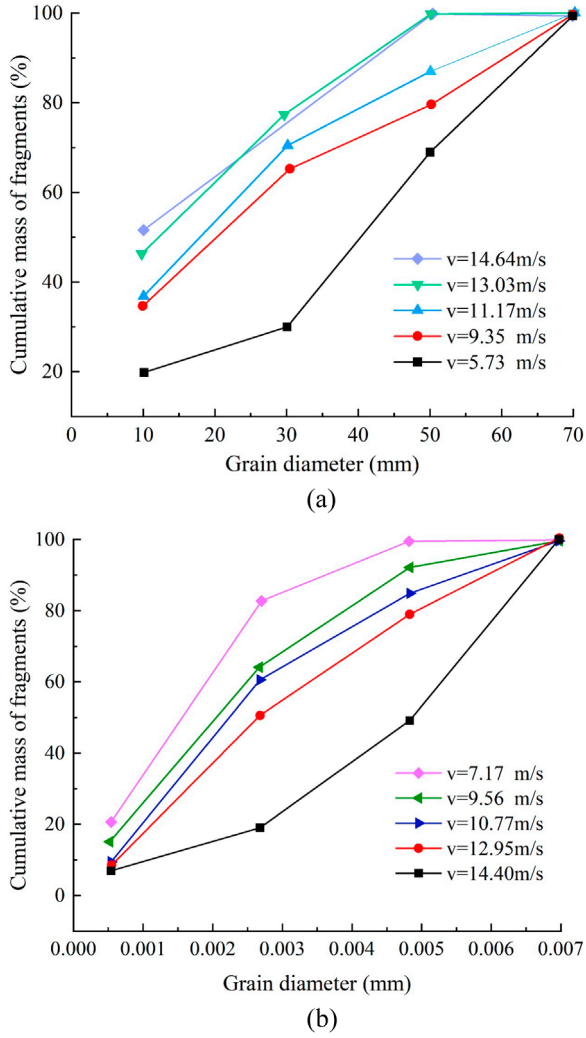

FIGURE 9
The fragmentation distribution of similar material specimens at various impact velocities: **(a)** Mudstone -like material, **(b)** Siltstone-like material.

rock failure block size with higher impact velocities. At lower impact speeds, only minimal energy is sufficient to cause slight fragmentation in the rock sample. However, as impact velocity rises, the degree of fragmentation intensifies and multiple occurrences of tensile shear failure result in the formation of macroscopic fracture surfaces. This further enhances the level of fragmentation within the rock samples and ultimately leads to decreased block sizes post-failure.

The fractal characteristics of rocks can provide insights into the fracture mechanism of rocks. To investigate the fracture mechanism of sandstone under varying impact rates, we employed a particle size classification method to conduct an in-depth analysis of the experimental observations. Specifically, we statistically measured the longest edge of broken rock fragments and weighed the accumulated mass of fragments across different particle sizes, establishing a relationship between these two variables. The fragmentation distribution patterns for mudstone and siltstone under different impact velocities are illustrated in Figure 9, while Figure 10 depicts the $ln\left[M_{(R)}/M_T\right] - lnR$ curve for a representative rock specimen. Additionally, we calculated the fractal dimension using formulas 10, 11 (Wu J. H. et al., 2024).

$$b = \frac{ln\left[\frac{M_{(R)}}{M_T}\right]}{lnR} \tag{10}$$

$$D = 3 - b \tag{11}$$

where b represents the slope of the fitting function in the double logarithmic coordinate system of $ln\left[M_{(R)}/M_T\right] - lnR$; $M_{(R)}$ represents the particle size less than R accumulated debris quality; M_T represents the sample quality; and D represents the fractal dimension of the sample fragments.

The fractal dimension of rock fragments increases as a quadratic function with the increase of impact velocity, as shown in Figure 11,

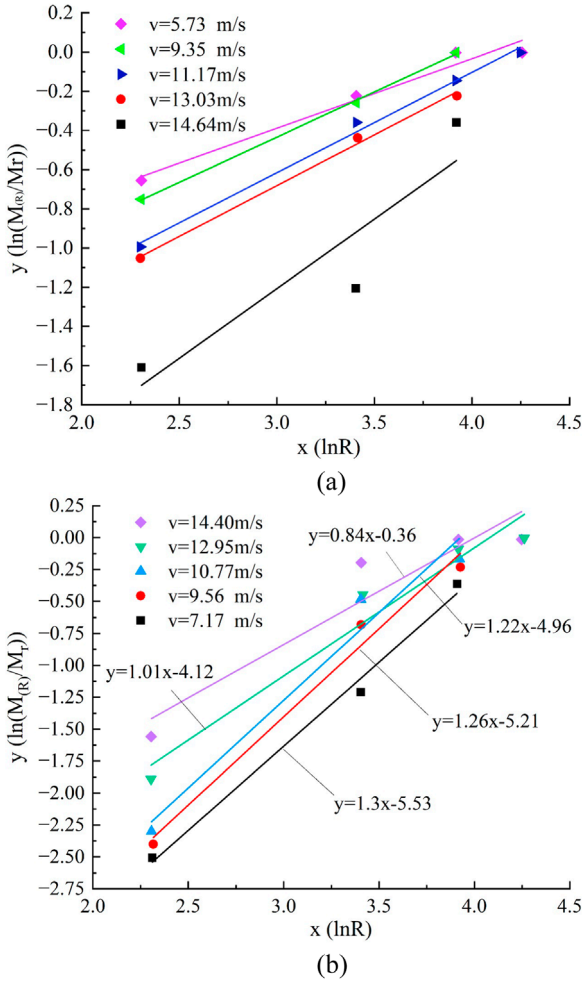

FIGURE 10
The $ln\left[M_{(R)}/M_T\right]$ – lnR curve of similar material specimens: **(a)** Mudstone -like material, **(b)** Siltstone-like material.

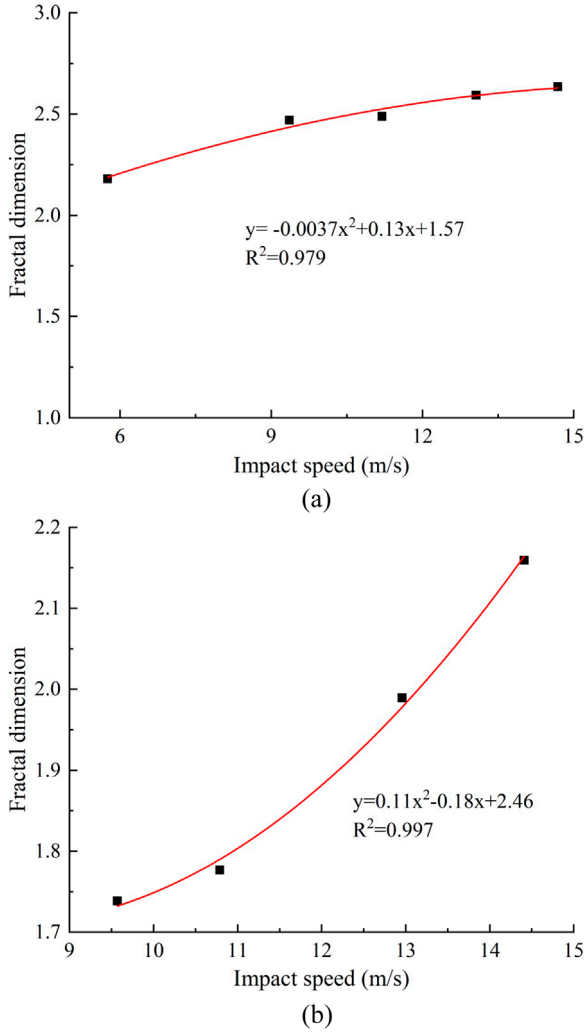

FIGURE 11
The typical relationship between the fractal dimension and dissipated energy of similar material specimens: **(a)** Mudstone -like material, **(b)** Siltstone-like material.

indicating that the fragmentation degree of mudstone and siltstone also increases correspondingly. Based on the macroscopic morphology analysis of typical rock breakage under different impact velocities, it can be concluded that higher impact velocities result in increased load and energy absorption by the rock sample, leading to enhanced crushing degree. Therefore, fractal dimension serves as a quantitative index for describing fracture characteristics and reflecting the extent of rock sample fractures. Through advanced drilling sampling and SHPB test analysis, the anticipated fractal dimensions of fractures in the roof rocks across various sections ahead of the roadway can be determined. Subsequently, by differentiating these fractal dimensions, support designs tailored to specific roof sections can be developed. This approach enables a more scientific alignment with the rock mass conditions, thereby achieving an optimal balance between safety and economic efficiency.

The relationship between the fractal dimension of rock sample fragments and dissipated energy exhibits an exponential pattern, as illustrated in Figure 12. As dissipated energy increases, the fractal dimension of rock progressively rises due to the absorption of energy during crack formation. Moreover, escalating impact velocity intensifies rock damage, necessitating a greater amount of absorbed energy for crack propagation until complete failure.

4 Conclusion

Based on the comprehensive experimental investigation using the Split Hopkinson Pressure Bar (SHPB) system and subsequent detailed analyses of mechanical response, failure modes, fragmentation, and energy dissipation, the following principal conclusions are drawn regarding the dynamic behavior of weakly cemented siltstone and mudstone:

(1) The two rock materials exhibit a pronounced strain rate effect, indicating an exponential increase in dynamic compressive strength and strain rate. Moreover, the dynamic compressive property of sandstone is significantly superior to that of

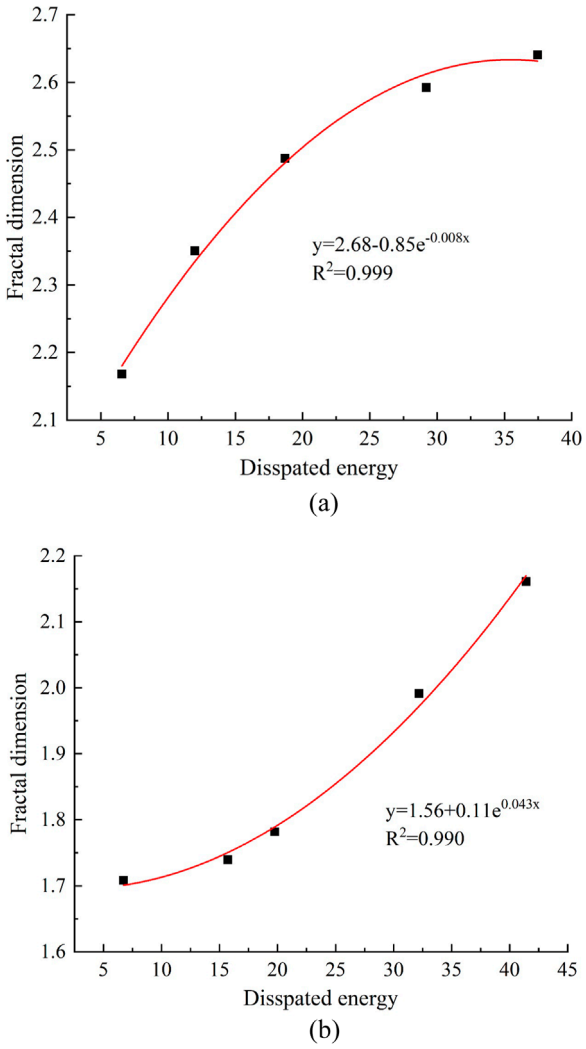

FIGURE 12
The relationship between the fractal dimension and dissipated energy of similar ma-terial specimens: **(a)** Mudstone -like material, **(b)** Siltstone-like material.

mudstone as the strain rate increases. At equivalent impact velocities, mudstone demonstrates greater ductility but lower yield strength compared to siltstone.

(2) Under low strain rates, the rock specimen exhibits splitting failure with a relatively mild degree of failure and maintains certain integrity. Typically, the specimen initially cracks from the side before experiencing complete failure. As the strain rate increases, the failure mode gradually transitions from splitting to crushing failure, resulting in a small but noticeable increase in fragment count. Additionally, siltstone fragments are significantly larger than mudstone materials. The fractal dimension of rock fragments under impact loads follows a quadratic function as impact velocity increases.

(3) With an increase in impact velocity of 9 m/s, the energy dissipation rate of mudstone exhibited a significant rise of 9.3%, from 13.5% to 24.8%. Similarly, the energy dissipation rate of siltstone also experienced a notable increase of 9.1%, from 18.1% to 27.2%.

Data availability statement

The original contributions presented in the study are included in the article/supplementary material, further inquiries can be directed to the corresponding author.

Author contributions

GS: Conceptualization, Writing – original draft, Methodology, Data curation. DY: Methodology, Writing – review and editing, Supervision, Funding acquisition, Resources, Project administration. JW: Validation, Writing – review and editing. FM: Data curation, Writing – review and editing.

Funding

The author(s) declare that financial support was received for the research and/or publication of this article. This work was funded by the University Synergy Innovation Program of Anhui Province (Grant No. GXXT-2021-016); the open Foundation of National-local joint Engineering Laboratory of building health monitoring and disaster prevention technology (GG23KF001); the Scientific Research Foundation for High-level Talents of Anhui University of Science and Technology (13210614); National Natural Science Foundation of China (Project No. 41977253).

Conflict of interest

The authors declare that the research was conducted in the absence of any commercial or financial relationships that could be construed as a potential conflict of interest.

Generative AI statement

The author(s) declare that no Generative AI was used in the creation of this manuscript.

Publisher's note

References

Chen, S. G., Zhang, H. M., Wang, L., Yuan, C., Meng, X. Z., Yang, G. S., et al. (2022). Experimental study on the impact disturbance damage of weakly cemented rock based on fractal characteristics and energy dissipation regulation. *Theor. Appl. Fract. Mech.* 122, 103665. doi:10.1016/j.tafmec.2022.103665

Cheng, B., Wang, Q., Wang, H., Zong, Q., and Gao, P. (2024). Research on the mechanism and application of wedge cutting blasting with hole-inner delay. *Sci. Rep.* 14 (1), 11383. doi:10.1038/s41598-024-62318-2

Deng, G., Xie, H., Gao, M., Xie, J., Li, C., and He, Z. (2023). Fracture mechanisms of competent overburden under high stress conditions: a case study. *Rock Mech. Rock Eng.* 56 (3), 1759–1777. doi:10.1007/s00603-022-03169-z

Fang, S., Yang, Y., Zhao, Y., Chen, J., and Li, W. (2023a). Dynamic mechanical properties and energy dissipation of frozen weakly cemented red sandstone under high strain rate loading. *Bull. Eng. Geol. Environ.* 82 (11), 418.

Fang, S. Z., Yang, Y., Zhao, Y., Chen, J., and Li, W. Y. (2023b). Dynamic mechanical properties and energy dissipation of frozen weakly cemented red sandstone under high strain rate loading. *Bull. Eng. Geol. Environ.* 82 (11), 418. doi:10.1007/s10064-023-03436-5

Gao, W., Li, J., Wang, C., and Feng, Y. T. (2024). Numerical investigation of impact fracture behaviors of rocks under confining pressure. *Int. J. Fract.* 245 (1-2), 37–56. doi:10.1007/s10704-023-00747-2

Gong, F., Dai, J., and Xu, L. (2023). A strength-stress coupling criterion for rockburst: inspirations from 1114 rockburst cases in 197 underground rock projects. *Tunn. Undergr. Space Technol.* 142, 105396. doi:10.1016/j.tust.2023.105396

Hao, Z., Sun, G., and Zhang, G. (2022). Mechanism and inducing factors of rockburst events of roadways under ultrathick strata. *Front. Earth Sci.* 10. doi:10.3389/feart.2022.860929

He, M. C., Wu, Y. Y., Gao, Y. B., and Tao, Z. G. (2024). Research progress of rock mechanics in deep mining. *J. China Coal Soc.* 49 (1), 75–99. doi:10.13225/j.cnki.jccs.2023.1400

Hu, J., He, M., Li, H., Cheng, T., Tao, Z., Liu, D., et al. (2023). Control effect of negative Poisson's ratio (NPR) cable on impact-induced rockburst with different strain rates: an experimental investigation. *Rock Mech. Rock Eng.* 56 (7), 5167–5180. doi:10.1007/s00603-023-03324-0

Kang, H. P., Gao, F. Q., Xu, G., and Ren, H. W. (2023). Mechanical behaviors of coal measures and ground control technologies for China's deep coal mines - a review. *J. Rock Mech. Geotechnical Eng.* 15 (1), 37–65. doi:10.1016/j.jrmge.2022.11.004

Li, C. X., Yang, R. S., Zuo, J. J., and Xie, P. (2025). Theory and field tests of innovative cut blasting method for rock roadway excavation, 155, 106180(1). doi:10.1016/j.tust.2024.106180

Li, S. S., and Yuan, L. (2023). Carbon emission accounting and influencing factors for whole life cycle of coal industry. *J. China Coal Soc.* 48 (7), 2925–2935. doi:10.13225/j.cnki.jccs.CN23.0368

Liao, Z. Q., Ding, X. H., Liang, M. Z., Li, J. F., Yang, Z. G., Liu, X., et al. (2025). Research on the optimization of optimal blasting parameters and fragmentation control based on coal seam geological conditions. *Sci. Rep.* 15 (1), 12238. doi:10.1038/s41598-025-94278-6

Liu, X., Liu, Y., Dai, F., and Yan, Z. (2022). Tensile mechanical behavior and fracture characteristics of sandstone exposed to freeze-thaw treatment and dynamic loading. *Int. J. Mech. Sci.* 226, 107405. doi:10.1016/j.ijmecsci.2022.107405

Lyu, P., Lu, K., and Chen, X. (2022). Mining stress distribution in stope and overlying rock fracture characteristics and its disaster-pregnant mechanism of coal mine earthquake. *Shock Vib.* 2022, 1–17. doi:10.1155/2022/7606360

Lyu, X. F., Lin, X., Wei, O. Y., Wang, N. J., and Zhang, F. R. (2023). Stress wave propagation attenuation law and energy dissipation characteristics of rock-barrier-coal composite specimen under dynamic load. *J. Central South Univ.* 30 (1), 276–288. doi:10.1007/s11771-023-5234-7

Meng, L. D., Han, L. J., Meng, Q. B., Liu, K. X., Tian, M. L., and Zhu, H. X. (2020). Study on characteristic and energy of argillaceous weakly cemented rock under dynamic loading by Hopkinson bar experiment. *Energies* 13 (12), 3215. doi:10.3390/en13123215

Rae, A. S. P., Kenkmann, T., Padmanabha, V., Poelchau, M. H., and Schafer, F. (2020). Dynamic compressive strength and fragmentation in felsic crystalline rocks. *J. Geophys. Research-Planets* 125 (10). doi:10.1029/2020je006561

Shi, H., Chen, W., Zhang, H., and Song, L. (2023b). A novel obtaining method and mesoscopic mechanism of pseudo-shear strength parameter evolution of sandstone. *Environ. Earth Sci.* 82 (2), 60. doi:10.1007/s12665-023-10748-y

Shi, H., Chen, W. L., Zhang, H. Q., Li, M., Wang, M. J. W., Lu, P. J., et al. (2023a). Dynamic strength characteristics of fractured rock mass. *Eng. Fract. Mech.* 292, 109678. doi:10.1016/j.engfracmech.2023.109678

Shi, H., Chen, W. L., Zhang, H. Q., Zhang, X. P., Song, L., Li, M., et al. (2025). Pull-out characteristics of rock bolts under the influence of "natural" coupled fractures. *Comput. Part. Mech.* 12, 1389–1409. doi:10.1007/s40571-024-00844-6

Shi, H., Zhang, H. Q., Chen, W. L., Song, L., and Li, M. (2024). Pull-out debonding characteristics of rockbolt with prefabricated cracks in rock: a numerical study based on particle flow code. *Comput. Part. Mech.* 11 (1), 29–53. doi:10.1007/s40571-023-00607-9

Shu, L., Yuan, L., Li, Q., Xue, W., Zhu, N., and Liu, Z. (2023). Response characteristics of gas pressure under simultaneous static and dynamic load: implication for coal and gas outburst mechanism. *Int. J. Min. Sci. Technol.* 33 (2), 155–171. doi:10.1016/j.ijmst.2022.11.005

Shu, R., Huang, L., Zhi, X., Han, Z., Lai, Y., Li, H., et al. (2022). Damage characteristic of thermal shock on the physical and dynamic compressive properties of granite. *Geofluids* 2022, 1–12. doi:10.1155/2022/1623883

Sun, B., Yang, P., Liu, S., and Zeng, S. (2023). Impact dynamic characteristics and constitutive model of granite damaged by cyclic loading. *J. Mater. Res. Technology-Jmr&T* 24, 333–345. doi:10.1016/j.jmrt.2023.03.047

Sun, L. H., Ji, H. G., and Yang, B. S. (2019). Physical and mechanical characteristic of rocks with weakly cemented stra-ta in Western representative mining area. *J. China Coal Soc.* 44 (3), 865–873. doi:10.13225/j.cnki.jccs.2018.6039

Tan, Y., Song, S., Zhang, X., and Liu, X. (2024). Safety evaluation method of bottom coal thickness in thick coal seam roadway. *Sci. Rep.* 14 (1), 14812. doi:10.1038/s41598-024-65708-8

Wang, C., Cheng, L. P., Tang, L. Z., Wang, W., Liu, T., Wei, Y. H., et al. (2019). Effects of the unloading rate on dynamic characteristic and failure modes of rock under high static loads. *Chin. J. Rock Mech. Eng.* 38 (2), 217–225. doi:10.13722/j.cnki.jrme.2018.0954

Wang, H., Xu, W., Cheng, B., and Zong, Q. (2023). Research on particle size and energy consumption law of hard coal crushing under impact load based on SHPB test. *Appl. Sciences-Basel* 13 (5), 3298. doi:10.3390/app13053298

Wang, H. P., Li, S. C., Zhang, Q. Y., Li, Y., and Guo, X. H. (2006). Development of a new geomechanical similar material. *Chin. J. Rock Mech. Eng.* 25 (09), 1842–1847. doi:10.3321/j.issn:1000-6915.2006.09.016

Wang, J., Zhu, C. G., Li, X., Wang, B., and Zhang, Y. T. (2024). Experimental study on triaxial disturbance and failure characteristics of rock-like specimens. *J. Min. Strata Control Eng.* 6 (2), 023034. doi:10.13532/j.jmsce.cn10-1638/td.20240015.004

Wang, J., Zuo, T., Li, X., Tao, Z., and Ma, J. (2021). Study on the fractal characteristics of the pomegranate biotite schist under impact loading. *Geofluids* 2021, 2021–2028. doi:10.1155/2021/1570160

Wang, S. M., Liu, L., Zhao, Y. J., Zhang, B., Wang, J. Y., Zhu, M. B., et al. (2022a). New energy exploitation in coal-endowed areas under the target of "double carbon": a new path for transformation and upgrading of coal mines in the future. *Coal Sci. Technol.* 51 (1), 59–79. doi:10.13199/j.cnki.cst.2022-2169

Wang, X., Zhu, Z., Zhou, L., Ma, L., Zhou, C., and Wang, Z. (2022b). Study on the effects of joints orientation and strength on failure behavior in shale specimen under impact loads. *Int. J. Impact Eng.* 163, 104162. doi:10.1016/j.ijimpeng.2022.104162

Wen, S., Huang, R., Zhang, C., and Zhao, X. (2023). Mechanical behavior and failure mechanism of composite layered rocks under dynamic tensile loading. *Int. J. Rock Mech. Min. Sci.* 170, 105533. doi:10.1016/j.ijrmms.2023.105533

Wu, H., Fan, A., Zheng, Z., Wang, M., Li, S., Zhang, B., et al. (2023). Dynamic mechanical properties and failure behaviors of brittle rock materials with a tunnel-shaped opening subjected to impact loads. *J. Mater. Res. Technology-Jmr&T* 25, 3285–3297. doi:10.1016/j.jmrt.2023.06.156

Wu, J. H., Du, Y. X., Wang, C. B., and Zong, Q. (2024b). Experimental study on dynamic tensile mechanical behavior and fracture mechanical characteristics of sandstone with a single prefabricated fissure. *Adv. Civ. Eng.* 2024, 2024. doi:10.1155/2024/5501703

Wu, J. Y., Wong, H. S., Zhang, H., Yin, Q., Jing, H. W., and Ma, D. (2024a). Improvement of cemented rockfill by premixing low-alkalinity activator and fly ash for recycling gangue and partially replacing cement. *Cem. Concr. Compos.* 145, 105345. doi:10.1016/j.cemconcomp.2023.105345

Wu, J. Y., Yang, S., Williamson, M., Wong, H. S., Bhudia, T., Pu, H., et al. (2025). Microscopic mechanism of cellulose nanofibers modified cemented gangue backfill materials. *Adv. Compos. Hybrid Mater.* 8, 177. doi:10.1007/s42114-025-01270-9

Xia, K., Yu, Y., Wu, B., and Yao, W. (2023). Correction of dynamic Brazilian disc tensile strength of rocks under preloading conditions considering the overload phenomenon and invoking the Griffith criterion. *J. Rock Mech. Geotechnical Eng.* 15 (8), 1986–1996. doi:10.1016/j.jrmge.2022.10.011

Xie, H. P., Lu, J., Li, C. B., Li, M. H., and Gao, M. Z. (2022). Experimental study on the mechanical and failure behaviors of deep rock subjected to true triaxial stress: a review. *Int. J. Min. Sci. Technol.* 32 (5), 915–950. doi:10.1016/j.ijmst.2022.05.006

Yang, R. S., Li, C. X. ; C. J., Zou, Fe. Y., Wang, Y. B., Xiao, C. L., and Zhang, Z. R. (2023). Development history and new technology research progress of rock roadway blasting excavation in coal mines in China. *Coal Sci. Technol.* 51 (1), 224–241. doi:10.13199/j.cnki.cst.2022-1804

Yang, S., Ning, J., Zhang, X., Wang, J., Shi, X., and Qu, X. (2024). Determination of critical energy for coal impact fracture under coupled static-dynamic loading. *Eng. Fail. Anal.* 160, 108222. doi:10.1016/j.engfailanal.2024.108222

Yin, Z., Wang, C., Chen, Z., Cao, Y., Yang, T., Chen, D., et al. (2024). Study on mechanical response characteristics of anchor under dynamic disturbance. *Archives Min. Sci.*, 69(1), 141–154. doi:10.24425/ams.2024.149833

You, W., Dai, F., Liu, Y., and Yan, Z. (2022). Effect of confining pressure and strain rate on mechanical behaviors and failure characteristics of sandstone containing a pre-existing flaw. *Rock Mech. Rock Eng.* 55 (4), 2091–2109. doi:10.1007/s00603-022-02772-4

Yuan, P., Zheng, X. B., Wei, N. N., and Li, A. B. (2024). Effect of impact loading and acidic drying-wetting cycles on fragmentation and energy dissipation characteristics of sandstone. *Environ. Earth Sci.* 83 (22), 632. doi:10.1007/s12665-024-11935-1

Yuan, Q., Wang, L., Xie, G., Gu, S., Khan, N. M., Jiao, Z., et al. (2022). Evaluation of the energy consumption and fractal characteristics of different length-diameter ratios of coal under dynamic impact. *Energies* 15 (15), 5498. doi:10.3390/en15155498

Yue, X., Tu, M., Li, Y., Chang, G., and Li, C. (2022). Stability and cementation of the surrounding rock in roof-cutting and pressure-relief entry under mining influence. *Energies* 15 (3), 951. doi:10.3390/en15030951

Zhang, Q. H., Yuan, L., Yang, K., Xue, J. H., and Duan, C. R. (2019). Mechanism analysis on continuous stress-relief mining for preventing coal and rock dynamic disasters in deep coal mines. *J. Min. and Saf. Eng.* 36 (1), 80–86+102. doi:10.13545/j.cnki.jmse.2019.01.012

Zhang, X., Liu, Z. G., Chang, S., Xue, Y. L., and Zhang, J. Y. (2025). Study on damage characteristics and fracture mechanisms of coal under high stress environment during blasting. *Eng. Fract. Mech.* 314, 110772. doi:10.1016/j.engfracmech.2024.110772

Zhang, Z., Qian, Q., Wang, H., Huang, Y., Wang, J., and Liu, H. (2021). Study on the dynamic mechanical properties of metamorphic limestone under impact loading. *Lithosphere* 2021 (Special 4), 8403502. doi:10.2113/2021/8403502

Zhao, H. B., Zhang, B., Gao, L., Jing, S. J., and Cheng, H. (2025). Static blasting roof cutting surrounding rock control technology for narrow coal pillar gob-side entry driving in thick coal seams. *Int. J. Geomechanics* 25 (6). doi:10.1061/IJGNAI.GMENG-10861

Zhao, Z., Xue, J., Jin, J., Tan, L., Xia, W., and Cai, R. (2023). Experimental research on the dynamic constringent characteristics and fractal properties of sandstone under impact loading. *Case Stud. Constr. Mater.* 18, e02174. doi:10.1016/j.cscm.2023.e02174

Zheng, Q., Qian, J., Zhang, H., Chen, Y., and Zhang, S. (2024a). Velocity tomography of cross-sectional damage evolution along rock longitudinal direction under uniaxial loading. *Tunn. Undergr. Space Technol.* 143, 105503.

Zheng, Q., Xu, Y., Yin, Z., Wang, F., and Zhang, H. (2023). Dynamic tensile behaviour under impact loading for rocks damaged by static precompression. *Archives Civ. Mech. Eng.* 23 (3), 199. doi:10.1007/s43452-023-00748-x

Zheng, Q. Q., Li, P. F., Xu, Y., Cheng, B., Hu, H., Shi, H., et al. (2025). Crack propagation and CT imaging of internal cracks in rocks damaged by pre-compression under explosive loading. *Ain Shams Eng. J.* 16 (3), 103302. doi:10.1016/j.asej.2025.103302

Zheng, Q. Q., Qian, J. W., Zhang, H. J., Chen, Y. K., and Zhang, S. H. (2024b). Velocity tomography of cross-sectional damage evolution along rock longitudinal direction under uniaxial loading. *Tunn. Undergr. Space Technol.* 143, 105503. doi:10.1016/j.tust.2023.105503

Zhou, J., Xu, W. S., Zhao, G. M., Meng, X. r., Li, Y. M., Wu, X. k., et al. (2022c). Energy evolution law and fractal characteristics of different rock specimen sizes on dynamic compression. *Geofluids* 2022, 1–10. doi:10.1155/2022/5339603

Zhou, K., Dou, L., Li, X., Song, S., Cao, J., Bai, J. Z., et al. (2022a). Coal burst and mining-induced stress evolution in a deep isolated main entry area - a case study. *Eng. Fail. Anal.* 137, 106289. doi:10.1016/j.engfailanal.2022.106289

Zhou, T., Han, Z., Li, D., and Chen, J. (2022b). Experimental study of the mechanical and fracture behavior of flawed sandstone subjected to coupled static-repetitive impact loading. *Theor. Appl. Fract. Mech.* 117, 103161. doi:10.1016/j.tafmec.2021.103161

Zhu, J., Hu, S., and Wang, L. (2009). An analysis of stress uniformity for concrete-like specimens during SHPB tests. *Int. J. Impact Eng.* 36 (1), 61–72. doi:10.1016/j.ijimpeng.2008.04.007

Zuo, T., Li, X., Wang, J., Hu, Q., Tao, Z., and Hu, T. (2024). Insights into natural tuff as a building material: effects of natural joints on fracture fractal characteristics and energy evolution of rocks under impact load. *Eng. Fail. Anal.* 163, 108584. doi:10.1016/j.engfailanal.2024.108584

Zuo, T., Zhao, Z., Wang, J., Li, X., Tao, Z., and Yang, C. (2022). Analysis of dynamic damage fractal and energy consumption characteristics of dolomite marble. *Shock Vib.* 2022, 1–11. doi:10.1155/2022/9440222